

Optimized Method for Selecting the Common Master Image in PS-InSAR Based on Error Analysis

Xiangtong Liu^{1,2,3}, Qiuxiang Cao^{2,4,*}, Zhuguo Xiong², Shengping Wang² and Chernyatyeva Anastasia⁵

¹School of Geoscience and Info-Physics Engineering, Central South University, Changsha 410083, China

²Department of Geomatics, East China University of Technology, Nanchang 330013, China

³Key Laboratory of Watershed Ecology and Geographical Environment Monitoring, NASG, Nanchang 330013, China

⁴State Key Laboratory Breeding Base of Nuclear Resources and Environment, East China Institute of Technology, Nanchang 330013, China

⁵Department of Geology, St. Petersburg State University, St. Petersburg 48202, Russia

Received 11 January 2018; Accepted 12 April 2018

Abstract

Permanent scatterer interferometric synthetic aperture radar (PS-InSAR) is a typical time series analysis technique. The selection of the common master image within the PS-InSAR influences the time series analysis. A novel method was proposed to extract the optimal common master image based on an error analysis of the observations. Tolerance and gross error were evaluated by calculating the root mean square errors (RMSEs) of effective spatio-temporal baselines and differences in Doppler centroid frequency of each interferogram sequence. Then, the interferogram sequence was optimized by setting the tolerance. After that, the RMSEs of each interferogram sequence with gross error removed were recalculated. Finally, the optimal common master image, which had the maximal sum of weights, was obtained after weighing the interferogram sequence with gross error removed. A case study was conducted to verify the rationality of selecting the common master image using 19 images of the European Remote Sensing Satellites-1/2. Results show that the common master images that are selected through the error analysis method are more optimized than that selected from the commonly used methods. The maximum of effective spatio-temporal baselines and difference in Doppler centroid frequency of the optimum interferometric pairs are 497, 910, and 222, respectively; the minimum are 149, 449, and 103, correspondingly, and the standard deviation values are 141, 299, and 55, respectively. In comparison with the common master image generated separately by the integrated correlation coefficient algorithm and the minimum sum of the three baseline algorithms, the values are reduced by 80, 0, 75, 12, 6, -14, 20, 13, and 47. Thus, the results show improved statistical properties. The outcome indicates that the error analysis method can be used to select the optimum common master image. The proposed method provides an effective approach to optimizing the common master image and presents a certain significance for selecting the common master image.

Keywords: Permanent scatter InSAR, Common master image, Error analysis

1. Introduction

Interferometric synthetic aperture radar (InSAR) is a microwave remote sensing surveying method. Compared with traditional methods of survey, InSAR is a unique tool for low-cost precise digital elevation model generation and large-coverage surface deformation monitoring with features of wide-range, all-weather, and high-precision [1-4]. Permanent scatterer interferometric synthetic aperture radar (PS-InSAR) technique is an advanced InSAR technology that is used to detect slow and long-term surface deformation. This technique can slightly overcome the temporal, spatial, and atmospheric phase screen decorrelations of the interferograms [5-9]. The PS-InSAR technology has been developed with the extensive application of SAR technology. Related works in preprocessing of data, selecting the common master image, and subsequent application of data have been conducted, especially the method for selecting the common master image [3, 10-13].

The selection of the common master image in the PS-InSAR widely and directly influences the quality of interferograms and the time series analysis about interferometric phase. The number of SAR images used in the PS-InSAR increases with the rapid development of SAR sensors and the accumulation in available SAR data. A reasonable selection of a common master image is important, especially for the SAR images with different characteristics. Furthermore, the implementation efficiency of the algorithm for selecting the common master image has been improved by applying high-performance computers in the PS-InSAR technology. The efficiency of traditional algorithms can also be improved.

Existing studies have mainly focused on the effect about quality of the interferogram sequence caused by selecting the common master image and the method for obtaining high-quality effective spatio-temporal baselines and differences in Doppler centroid frequency of each interferogram sequence. Several other researchers have mainly considered prior information, such as specific experimental areas and methods, but have disregarded the selection method of the common master image [14, 15]. Most studies on selecting the common master image have

*E-mail address: tomcleck@126.com

focused on the final quality of the interferogram and application area. However, only a few observations on the characteristics of effective spatio-temporal baselines and differences in Doppler centroid frequency of interferogram sequences have been obtained.

Owing to the analysis presented previously, an idea based on an error analysis of the observation values was used to examine the inherent characteristics of effective spatio-temporal baselines and differences in Doppler centroid frequency. Then, the optimum common master image and interferogram sequence with superior quality were obtained.

2. State of the art

The selection of the common master image is an important part of the PS-InSAR technique, and the result of the selection directly affects the coherence of the interferogram sequence. The problem of selecting the common master image was discussed when the PS-InSAR technology was proposed by Ferretti et al. [1, 5]. The temporal baseline of 3 years was used as a constraint to generate interferometric pairs (refer to the European Remote Sensing Satellite [ERS] case) to reduce the influence of decorrelation. Afterward, the selection method of the common master image restricted by temporal baseline has been used and improved continuously. This technique is simple and easy but fails to analyze the basis of selecting the common master image.

Zebker et al. [16] first conducted a systematic study on the causes of the decorrelation about interferometric pairs. The findings indicated that temporal baseline, effective spatial baseline, and thermal noise were the main factors that affected the decorrelation of interferometric pairs, which should be considered in generating interferometric pairs. Difference in Doppler centroid frequency was considered as main part of thermal noise by Hooper et al. [10] when they used the PS-InSAR to study volcanic deformation. They thought that the noise could be removed by filtering, except for the difference of Doppler centroid frequency. One scene was selected as the common master image (based primarily on minimization of effective spatial baseline and secondarily on minimization of temporal baseline) and created 21 interferograms. The method demonstrated the effectiveness for discussing volcanic deformation, fault slip, landslides, and subsidence. Kampes et al. [17–19] adopted the temporal and effective spatial baselines to improve the selection of the common master image. The accuracy increased when calculating the settlement of permanent scatterers (PS) with a least square method. However, the possibilities of other factors were disregarded. Further relevant research based on this method has been conducted [20, 21]. Thus, temporal and effective spatial baselines were used as the selection methods of common master image by Zhang et al. [22]. The influences of the difference in Doppler centroid frequency and terrestrial vegetation change at different times in the common master image were also analyzed. Chen et al. [11] applied the integrated correlation coefficient algorithm to select the common master image. The temporal baseline, effective spatial baseline, and difference in Doppler centroid frequency were simultaneously considered in this model. The selection of the common master image was determined by the maximum correlation coefficient, which can be used to decide on the optimum images. The minimum sum of baselines was used by Tao et al. [14] to improve optimization efficiency. However, analyzing the baseline in

the algorithm was simple because the rights of the individual effects of the baseline weight were ignored. Wang et al. [23] adopted the method for equal influence to measure the effect of various factors. This technique is stable when individual data quality is satisfactory. However, this technique is unsuitable when individual data quality is poor. Luo et al. [24] and Pan et al. [25] used image clustering and orthogonal characteristics to select the common master image from the mathematical perspective. Liu et al. [26] mapped all of the elements into a 3D space and selected the common master image by locating the space centroid. The two approaches can determine the common master image with definite physical properties. However, the process is complex, and the unique features of the interferograms was disregarded. Long et al. [12] utilized a priori information of external global positioning system (GPS) data to select the common master image; however, the GPS data are not constantly available. Rosi et al. [4] utilized a priori information of landslides to select the common master image in investigating landslides. Liu et al. [27] selected the common master image by using the theory of surveying adjustment to weigh the relationship between temporal baseline, effective spatial baseline, and difference in Doppler centroid frequency of each interferogram sequence but disregarded the features of each factor (i.e., temporal baseline, effective spatial baseline, and difference in Doppler centroid frequency).

The selected results do not guarantee optimality because existing methods disregard the characteristics of the effective spatio-temporal baselines and difference in Doppler centroid frequency of each interferogram sequence. The present proposes an optimization selection model based on error analysis theory, which considers the comprehensive effects of various factors and have the ability to select the optimized common master image. First, the tolerance is obtained by calculating the root mean square errors (RMSEs) of the effective spatio-temporal baselines and differences in Doppler centroid frequency of each interferogram sequence. Then, the tolerance is used as a threshold to optimize the interferogram sequence. If the error of factors in the interferogram sequence is greater than the tolerance (gross error), then its weight is assigned with 0. Furthermore, the RMSEs of the temporal baselines, effective spatial baselines, and differences in Doppler centroid frequency of each interferogram sequence without gross error are recalculated. Finally, the optimum common master image that has the maximum sum of weights is obtained after weighing the interferogram sequence without gross error.

The remainder of this study is organized as follows: The basic concepts of RMSE, tolerance, gross error detection, and weight are described in Section 3. The procedure for selecting the common master image using the error analysis algorithm is also discussed. An application example of the error analysis method is introduced in Section 4. The statistical characteristics of the common master image selected by this technique are also analyzed. The conclusions drawn from this study are presented in Section 5.

3. Methodology

3.1 RMSE, tolerance, gross error detection, and weight

In the theory of surveying adjustment, the RMSE is an absolute numerical characteristic of accuracy. A definite RMSE is derived when certain observation conditions exhibit relative error distributions. Given the characteristics

of the interferometric results, the interferogram sequence is evaluated using the RMSE.

For a group of n independent and equal-precision observations (X_1, \dots, X_n) , the formula of the RMSE in the observations is expressed as follows:

$$m_i = \sqrt{\frac{\sum_{i=1}^n (X_i - \bar{X})^2}{n-1}}, \quad (1)$$

where m_i is the RMSE of the observed value, and \bar{X} is the mean of the observed value (X_1, \dots, X_n) .

Tolerance is the limit of the absolute value of the measurement error under certain observation conditions. Typically, two to three times of the RMSE are used as the values of tolerance. The observation, which error value is greater than the tolerance, is considered inaccurate and is called gross error. The process of obtaining the gross error is called gross error detection. Thus, the interferometric pair in the interferogram sequence with poor quality can be removed by the gross error detection.

In comparing the accuracy among various observations, the precision of the observed values is determined using the proportional relationship among RMSEs. The digital signature that represents the proportional relationship of each observation variance is called weight, that is, a relative numerical characteristic to represent accuracy.

For a group of equal-precision observations,

$$P = \frac{\sigma_0^2}{\sigma_i^2}, \quad (2)$$

where P is the weight of the observed value, σ_0^2 is the variance of the unit weight, and σ_i^2 is the square of the RMSE of an observation.

The quality of the interferogram sequences can be clearly evaluated by weighing the effective spatio-temporal baselines and differences in Doppler centroid frequency of each interferometric pair.

3.2 Error analysis algorithm and calculation process

The temporal baselines, effective spatial baselines, and differences in Doppler centroid frequency are regarded as three groups of independent equal-precision observations. The RMSEs and tolerance of each interferogram sequence are solved. The interferometric pair, which error is greater than the tolerance, should be removed by using the method for gross error detection and weighed as 0 (the “master” image in the removed interferometric pair is not considered an option for the common master image). Then, the RMSEs of the effective spatio-temporal baselines, and differences in Doppler centroid frequency of each interferogram sequence without gross error are recalculated. The optimum common master image, which has the maximum sum of weights, is obtained after weighing the interferogram sequence without gross error. This method is called error analysis.

N interferometric pairs consist of n images, which include a pair composed of the image and itself when one image is selected as the common master image. The error analysis is conducted when the i th image is selected as the common master image, as follows:

1) The interferogram sequence is composed of the common master image with i th image, and the RMSEs of the temporal baselines, effective spatial baselines, and differences in Doppler centroid frequency are calculated separately as follows:

$$m_{T_i} = \sqrt{\frac{\sum_{i=1}^n (T_i - \bar{T})^2}{n-1}}, \quad (3)$$

where m_{T_i} is the RMSE of the temporal baseline, T_i is the temporal baseline, \bar{T} is the mean of the temporal baseline, and n is the number of image pairs;

$$m_{B_i} = \sqrt{\frac{\sum_{i=1}^n (B_i - \bar{B})^2}{n-1}}, \quad (4)$$

where m_{B_i} is the RMSE of the effective spatial baseline, B_i is the effective spatial baseline, \bar{B} is the mean of the effective spatial baseline, and n is the number of image pairs;

$$m_{D_i} = \sqrt{\frac{\sum_{i=1}^n (D_i - \bar{D})^2}{n-1}}, \quad (5)$$

where m_{D_i} is the RMSE of the Doppler centroid frequency difference, D_i is the Doppler centroid frequency difference, \bar{D} is the mean of the Doppler centroid frequency difference, and n is the number of image pairs.

2) The interferometric pair with gross error is removed using the theory of tolerance and gross error detection. Then, the RMSEs of the effective spatio-temporal baselines and differences in Doppler centroid frequency of each interferogram sequence without gross error are recalculated (the “master” image in the removed interferometric pair is not considered as an option for the common master image). The gross error detection of the temporal baseline, effective spatial baseline, and difference in Doppler centroid frequency are calculated separately as follows:

$$T_i = \begin{cases} P_{T_i} = 0 & \left| |T_i| - |T_{i,average}| \right| \geq 2m_{T_i} \\ T_i & \left| |T_i| - |T_{i,average}| \right| < 2m_{T_i} \end{cases}, \quad (6)$$

where P_{T_i} is the weight of m_{T_i} , $|T_i|$ is the absolute value of the temporal baseline, and $|T_{i,average}|$ is the mean of the absolute value of the temporal baseline;

$$B_i = \begin{cases} P_{B_i} = 0 & \left| |B_i| - |B_{i,average}| \right| \geq 2m_{B_i} \\ B_i & \left| |B_i| - |B_{i,average}| \right| < 2m_{B_i} \end{cases}, \quad (7)$$

where P_{B_i} is the weight of m_{B_i} , $|B_i|$ is the absolute value of the effective spatial baseline, and $|B_{i,average}|$ is the mean of the absolute value of the effective spatial baseline;

$$D_i = \begin{cases} P_{D_i} = 0 & \left| |D_i| - |D_i|_{average} \right| \geq 2m_{D_i} \\ D_i & \left| |D_i| - |D_i|_{average} \right| < 2m_{D_i} \end{cases}, \quad (8)$$

where P_{D_i} is the weight of m_{D_i} , $|D_i|$ is the absolute value of the Doppler centroid frequency difference, and $|D_i|_{average}$ is the mean of the absolute value of the difference in Doppler centroid frequency.

The assuming is that k interferograms are retained after removing the interferometric pair with gross error. The new RMSEs of the temporal baselines, effective spatial baselines, and differences in Doppler centroid frequency are calculated separately as follows:

$$m'_{T_i} = \sqrt{\frac{\sum_{i=1}^k (T_i - \bar{T}')^2}{k-1}}, \quad (9)$$

where m'_{T_i} is the new RMSE of the temporal baseline, T_i is the temporal baseline, \bar{T}' is the mean of the temporal baseline of the k image pairs, and k is the number of image pairs;

$$m'_{B_i} = \sqrt{\frac{\sum_{i=1}^k (B_i - \bar{B}')^2}{k-1}}, \quad (10)$$

where m'_{B_i} is the new RMSE of the effective spatial baseline, B_i is the effective spatial baseline, \bar{B}' is the mean of the effective spatial baseline of the k image pairs, and k is the number of image pairs;

$$m'_{D_i} = \sqrt{\frac{\sum_{i=1}^k (D_i - \bar{D}')^2}{k-1}}, \quad (11)$$

where m'_{D_i} is the new RMSE of the difference in Doppler centroid frequency, D_i is the difference in Doppler centroid frequency, \bar{D}' is the mean of the difference in Doppler centroid frequency of the k image pairs, and k is the number of image pairs.

3) The weights of the new RMSEs of the interferogram sequence, which use the i th image as common master image, can be derived alone using the numerical results of m'_{T_i} , m'_{B_i} , and m'_{D_i} . The weights of m'_{T_i} , m'_{B_i} , and m'_{D_i} can be obtained as follows:

$$P_{T_i} = \frac{m_{T_0}^2}{m'_{T_i}{}^2}, \quad (12)$$

where P_{T_i} is the weight of m'_{T_i} , and $m_{T_0}^2$ is the variance of the unit weight of the temporal baseline;

$$P_{B_i} = \frac{m_{B_0}^2}{m'_{B_i}{}^2}, \quad (13)$$

where P_{B_i} is the weight of m'_{B_i} , and $m_{B_0}^2$ is the variance of the unit weight of the effective spatial baseline;

$$P_{D_i} = \frac{m_{D_0}^2}{m'_{D_i}{}^2}, \quad (14)$$

where P_{D_i} is the weight of m'_{D_i} , and $m_{D_0}^2$ is the variance of the unit weight of the difference in Doppler centroid frequency.

4) The sum of weights of the interferogram sequence, which use the i th image as the common master image, can be determined as follows:

$$P_i = P_{D_i} + P_{B_i} + P_{T_i} \quad (15)$$

where P_{D_i} , P_{B_i} , and P_{T_i} are the weights of m'_{D_i} , m'_{B_i} , and m'_{T_i} , respectively; and P_i is the sum of weights of the interferogram sequence of the common master image with the i th image.

The flowchart of the calculation process is illustrated in Figure 1.

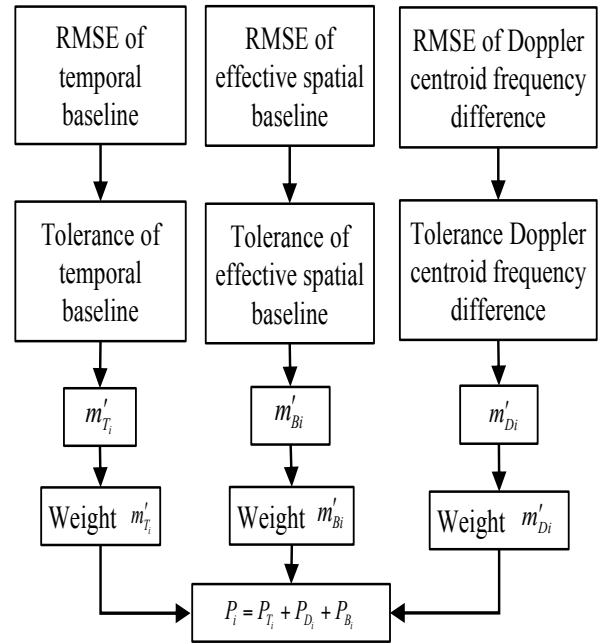


Fig. 1. Flowchart for computing the error analysis

4 Result analysis and discussion

Nineteen single-look complex images from the ERS-1/2 SAR sensor were acquired as examples (data from Tao et al. [14]) to examine the error analysis algorithm and the results of the selection method.

Table 1. Statistics of temporal baseline about interferograms (unit: day)

Image	1	2	3	4	5	6	7	8	9	10	11	12	13	14	15	16	17	18	19
1	0	35	70	140	315	350	490	700	804	805	909	910	1085	1120	1190	1400	1470	1645	1715
2	-35	0	35	105	280	315	455	665	769	770	874	875	1050	1085	1155	1365	1435	1610	1680
3	-70	-35	0	70	245	280	420	630	734	735	839	840	1015	1050	1120	1330	1400	1575	1645
4	-140	-105	-70	0	175	210	350	560	664	665	769	770	945	980	1050	1260	1330	1050	1575
5	-315	-280	-245	-175	0	35	175	385	489	490	594	595	770	805	875	1085	1155	1330	1400
6	-350	-315	-280	-210	-35	0	140	350	454	455	559	560	735	770	840	1050	1120	1295	1365
7	-490	-455	-420	-350	-175	-140	0	210	314	315	419	420	595	630	700	910	980	1155	1225
8	-700	-665	-630	-560	-385	-350	-210	0	104	105	209	210	385	420	490	700	770	945	1015
9	-804	-769	-734	-664	-489	-454	-314	-104	0	1	105	106	281	316	386	596	666	841	911
10	-805	-770	-735	-665	-490	-455	-315	-105	-1	0	104	105	280	315	385	595	665	840	910
11	-909	-874	-839	-769	-594	-559	-419	-209	-105	-104	0	1	176	211	281	491	561	736	806
12	-910	-875	-840	-770	-595	-560	-420	-210	-106	-105	-1	0	175	210	280	490	560	735	805
13	-1085	-1050	-1015	-945	-770	-735	-595	-385	-281	-280	-176	-175	0	35	105	315	385	560	630
14	-1120	-1085	-1050	-980	-805	-770	-630	-420	-316	-315	-211	-210	-35	0	70	280	350	525	595
15	-1190	-1155	-1120	-1050	-875	-840	-700	-490	-386	-385	-281	-280	-105	70	0	210	280	455	525
16	-1400	-1365	-1330	-1260	-1085	-1050	-910	-700	-596	-595	-491	-490	-315	-280	-210	0	70	245	315
17	-1470	-1435	-1400	-1330	-1155	-1120	-980	-770	-666	-665	-561	-560	-385	-350	-280	-70	0	175	245
18	-1645	-1610	-1575	-1505	-1330	-1295	-1155	-945	-841	-840	-736	-735	-560	-525	-455	-245	-175	0	70
19	-1715	-1680	-1645	-1575	-1400	-1365	-1225	-1015	-911	-910	-806	-805	-630	-595	-525	-315	-245	-70	0

*Temporal baselines are calculated using the acquisition time of the master image minus that of the slave image. Thus, negative temporal baselines exist.

Table 2. Statistics of difference in Doppler centroid frequency about interferograms (unit: HZ)

Image	1	2	3	4	5	6	7	8	9	10	11	12	13	14	15	16	17	18	19
1	0	-40	-13	-12	-64	6	59	-5	282	91	250	17	25	-23	63	-44	-15	313	157
2	40	0	27	28	-23	47	99	35	323	131	290	57	65	17	103	4	26	354	198
3	13	-27	0	1	-50	20	72	8	296	104	263	30	38	-10	76	-31	-1	327	171
4	12	-28	-1	0	-52	18	71	7	294	103	262	29	37	-11	75	-32	-3	325	169
5	64	23	50	52	0	70	122	59	346	155	313	81	89	41	127	20	49	377	221
6	-6	-47	-20	-18	-70	0	52	-12	276	84	241	10	19	-29	57	-50	-21	307	151
7	-59	-99	-72	-71	-122	-52	0	-64	224	32	191	-42	-34	-82	4	-103	-73	255	99
8	5	-35	-8	-7	-59	12	64	0	288	96	255	22	30	-18	68	-39	-10	318	162
9	-282	-323	-296	-294	-346	-276	-224	-288	0	-192	-33	-266	-256	-305	-219	-326	-297	31	-125
10	-91	-131	-104	-103	-155	-84	-32	-96	192	0	159	-73	-66	-114	-28	-135	-105	222	67
11	-250	-290	-263	-262	-313	-241	-191	-255	33	-159	0	-232	-225	-272	-186	-293	-264	64	-92
12	-17	-57	-30	-29	-81	-10	42	-22	266	73	232	0	8	-40	-3	64	288	297	141
13	-25	-65	-38	-37	-89	-19	34	-30	256	66	225	-8	0	-48	38	-69	-40	288	132
14	23	-17	10	11	-41	29	82	18	305	114	272	40	48	0	86	-21	8	336	97
15	-63	-103	-76	-75	-127	-57	-4	-68	219	28	186	3	-38	-86	0	-107	-78	250	94
16	44	-4	31	32	-20	50	103	39	326	135	293	61	69	21	107	0	29	357	201
17	15	-26	1	3	-49	21	73	10	297	105	264	31	40	-8	78	-29	0	328	172
18	-313	-354	-327	-325	-377	-307	-255	-318	-31	-222	-64	-296	-288	-336	-250	-357	-328	0	-156
19	-157	-198	-171	-169	-221	-151	-99	-162	125	-67	92	-141	-180	-97	-94	-201	-172	156	0

*Differences in Doppler centroid frequency are calculated using the value of the master image minus that of the slave image. Thus, negative Doppler centroid frequency differences exist.

Table 3. Statistics of effective spatial baseline about interferograms (unit: meter)

Image	1	2	3	4	5	6	7	8	9	10	11	12	13	14	15	16	17	18	19
1	0	446	151	17	124	86	673	-287	217	176	179	96	302	56	93	160	384	393	399
2	-446	0	-295	-429	-322	-360	227	-733	-229	-270	-267	-350	-144	-390	-353	-286	-62	-53	-47
3	-151	295	0	-134	-27	-65	522	-438	66	25	28	-55	151	-95	-58	9	233	242	248
4	-17	429	134	0	107	69	656	-304	200	159	162	79	285	39	76	143	367	376	382
5	-124	322	27	-107	0	-38	549	-411	93	52	55	-28	178	-68	-31	36	260	269	275
6	-86	360	65	-69	38	0	587	-373	131	90	93	10	216	-30	7	74	298	307	313
7	-673	-227	-522	-656	-549	-587	0	-960	-456	-497	-494	-577	-371	-617	-580	-513	-289	-280	-274
8	287	733	438	304	411	373	960	0	504	463	466	383	589	343	380	447	671	680	686
9	-217	229	-66	-200	-93	-131	456	-504	0	-41	-38	-121	85	-161	-124	-57	167	176	182
10	-176	270	-25	-159	-52	-90	497	-463	41	0	3	-80	126	-120	-83	-16	208	217	223
11	-179	267	-28	-162	-55	-93	494	-466	38	-3	0	83	123	-123	-86	-19	205	214	220
12	-96	350	55	-79	28	-10	577	-383	121	80	83	0	206	-40	-3	64	288	297	303
13	-302	144	-151	-285	-178	-216	371	-589	-85	-126	-123	-206	0	-246	-209	-142	82	91	97
14	-56	390	95	-39	68	30	617	-343	161	120	123	40	246	0	37	104	328	337	343
15	-93	353	58	-76	31	-7	580	-380	124	83	86	3	209	-37	0	67	291	300	306
16	-160	286	-9	-143	-36	-74	513	-447	-57	16	19	-64	142	-104	-67	0	224	233	239
17	-384	62	-233	-367	-260	-298	289	-671	-167	-208	-205	-288	-82	-328	-291	-224	0	9	15
18	-393	53	-242	-376	-269	-307	280	-680	-176	-217	-214	-297	-91	-337	-300	-233	-9	0	6
19	-399	47	-248	-382	-275	-313	274	-686	-182	-223	-806	-220	-303	-97	-343	-306	-239	-15	-60

*Effective spatial baselines are calculated using the perpendicular baseline of the master image minus that of the slave image. Thus, negative effective spatial baselines exist.

Following the model of the integrated correlation coefficient proposed by Chen et al.[10,11], the coefficients are assigned with 1 in the current study to select exponential values without significantly affecting the result[14]. The

results of error analysis, minimum sum of the three baselines, and integrated correlation coefficient are depicted in Figure 2.

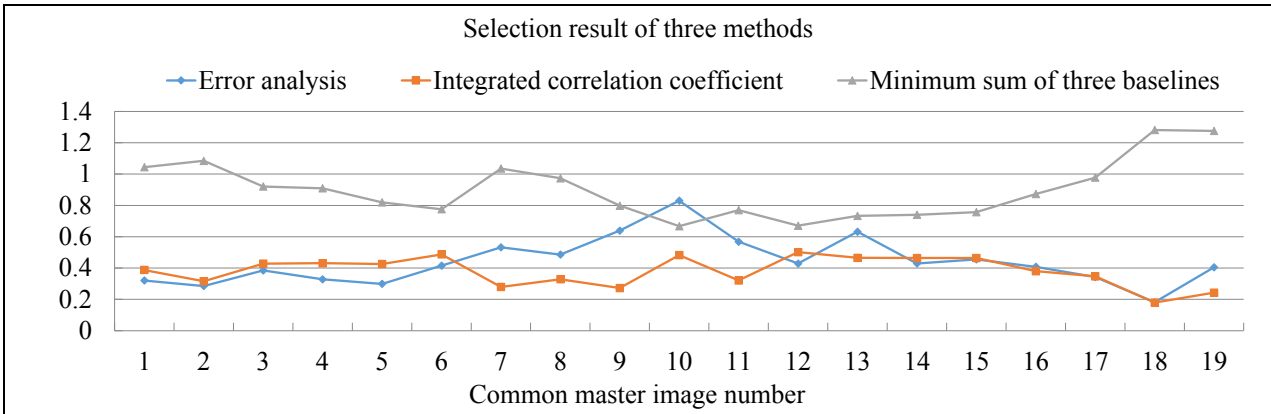


Fig. 2. Results of with error analysis, minimum sum of the three baselines, and integrated correlation coefficient

In Figure 2, the selection results are considerably better when computed by the error analysis model than by the integrated correlation coefficient and minimum sum of the three baseline models. The interferogram sequence with a gross error is shielded by the error analysis model in selecting the common master image, and the effect of the gross error on the results is minimized. The three components are listed separately in Figure 3 to illustrate the

situation of the three factors of the error analysis model. Figure 3 demonstrates that the weight of each component has different effects on the total weight. Clearly, the weight of the time baseline combinations is greater near the middle of the line chart. The characteristics of the weights of the effective spatial baseline and difference in Doppler centroid frequency combinations are not evident.

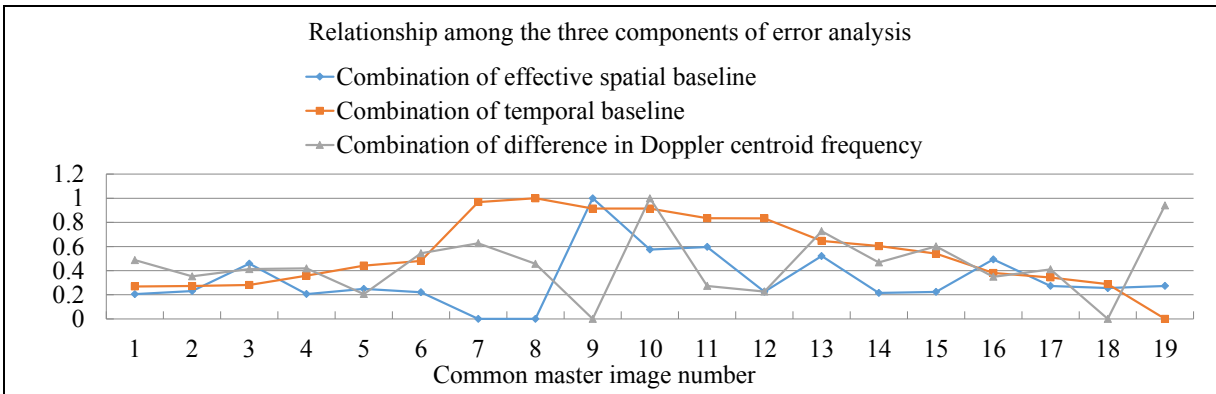


Fig. 3. Relationship among the three components of error analysis

The results of the integrated correlation coefficient model in the top three combinations of serial numbers are Groups 12, 6, and 10, and the results of the minimum sum of the baseline model in the top three combinations of serial numbers are Groups 12, 10, and 13.

The results calculated by the error analysis model in the top three combinations of serial numbers are Groups 10, 9, and 13. However, the “master” image in the interferometric pair with gross error cannot be an option for the common master image. Groups 9 should be weighed as zero and rejected because of gross error. . Significantly large values caused the decorrelation of the interferometric pairs, such as the effective spatial baselines of Groups 7 and 8 and the differences in Doppler centroid frequency of Groups 9 and 18 in Figure 3. Therefore, the results of the error analysis model in the top two combinations of serial numbers are Groups 10 and 13.

The selection by using these models is displayed in Table 4.

Table 4. Optimum common master image selected by using the three models

Model	First choice	Second choice	Third choice
Integrated correlation coefficient model	12	6	10
Minimum sum of baselines model	12	10	13
Error analysis model	10	9(Reject)	13

Groups 10 and 12 are utilized for optimum selection. For comparison, the temporal baseline, effective spatial baseline, and difference in Doppler centroid frequency combinations in Groups 10 and 12 are analyzed. The results are exhibited in Figure 4.

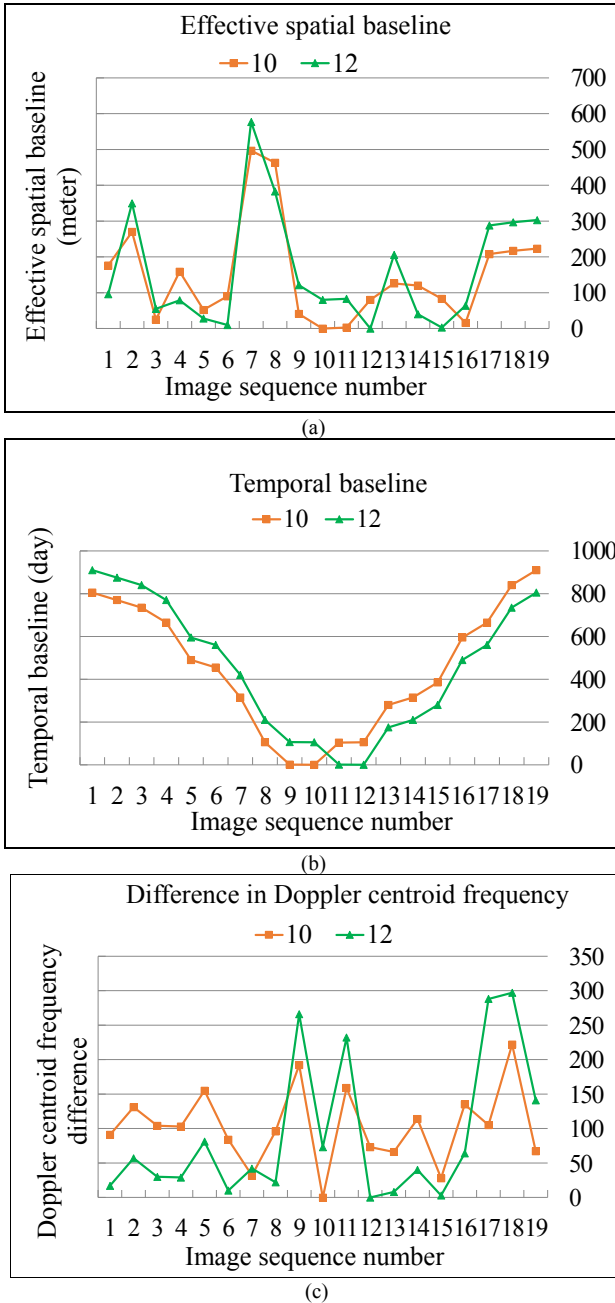


Fig. 4. Comparison among effective spatial baselines, temporal baselines, and differences in Doppler centroid frequency of Groups 10 and 12 SAR images

The comparison results of the combinations of Groups 10 and 12 indicate that Dataset 10 demonstrates better maximum and stability values than Dataset 12 in the effective spatial baseline (Figure 4a). Moreover, no obvious distinctions are observed between Datasets 10 and 12 in the temporal baselines (Figure 4b). Group 10 exhibits considerably better maximum value than Group 12. Furthermore, the maximum value is obviously less in Group 10 than in Group 12 in the differences of Doppler centroid frequency. The values of the differences in Doppler centroid frequency in Images 1–8 are slightly large.

The results of the quantitative analysis of the statistical information in Combinations 10 and 12 are listed in Table 5. Only the value of the difference in Doppler centroid frequency is larger in Combination 10 than in Combination 12; the remaining values are considerably enhanced. This result can be due to Combination 10 is more optimized than

Combination 12. Therefore, Combination 10 can be prioritized in selecting the common master image.

Table 5. Baseline statistics of Combinations 10 and 12

Influencing factors	Image number	Max	Min	Standard deviation
Temporal baseline	10	910	449	299
	12	910	455	312
difference in Doppler centroid frequency	10	222	103	55
	12	297	89	102
Effective spatial baseline	10	497	149	141
	12	577	161	161

The second option in the integrated correlation coefficient model is Combination 6. For comparison, the temporal baseline, effective spatial baseline, and difference in Doppler centroid frequency combinations in Groups 6, 10, and 9(which was rejected) are displayed in Figure 5.

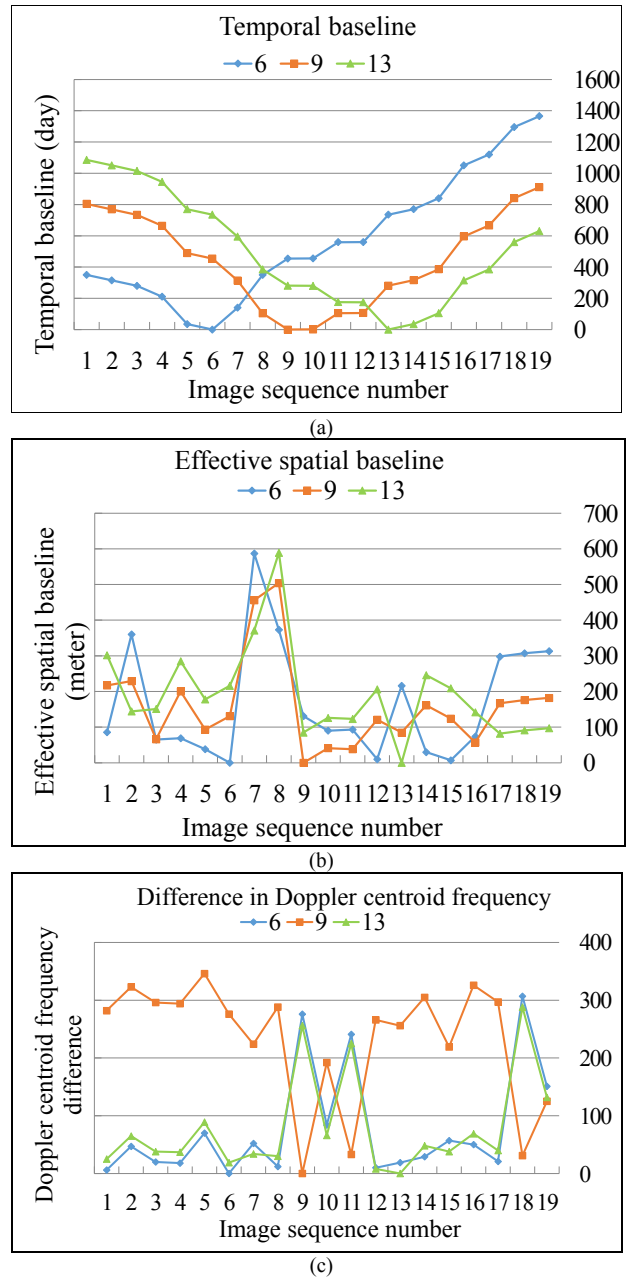


Fig. 5. Comparison among effective spatial baselines, temporal baselines, and differences in Doppler centroid frequency of Groups 6, 9 and 13 SAR images

The comparison of Datasets 6, 9, and 13 presented in Figure 5a indicates that Combinations 9 and 13 are superior to Combination 6 in terms of the temporal baseline. In addition, Combination 9 is better than Combinations 6 and 13 in terms of the effective spatial baseline. However, Combination 9 is more unstable and volatile than Combinations 13 and 6 in terms of the difference in Doppler centroid frequency (Figure 5c). Thus, Combination 9 is unsuitable for selecting the common master image and should be rejected.

For the quantitative analysis, the statistical information of the three combinations is listed in Table 6. Combination 13 has six values, which are smaller than those of Combination 6. This result can be due to Combination 13 is more optimized than Combination 6. Therefore, Group 13 can be prioritized in selecting the secondary common master image.

Table 6. Baseline statistics of Combinations 6, 9 and 13

Influencing factors	Image number	Max	Min	Standard deviation
Temporal baseline	6	1365	572	410
	9	911	449	299
	13	1085	501	353
difference in Doppler centroid frequency	6	307	77	95
	9	346	230	106
	13	288	79	84
Effective spatial baseline	6	587	165	162
	9	504	160	130
	13	589	191	131

5. Conclusions

The selection of the common master image directly influences the quality of the interferograms generated by a PS-InSAR. A novel method based on an error analysis was developed in this study to select the optimum common master image. The effective spatio-temporal baselines and difference in Doppler centroid frequency combinations were regarded as equal-precision observations. The method for gross error detection was adopted to optimize the interferogram sequence. Then, the weight was calculated. The optimum interferogram sequence with maximum weight could be selected. The following conclusions were drawn from this study:

(1) Due to the influences of the temporal baseline, effective spatial baseline, and difference in Doppler centroid frequency are considered comprehensively, an optimized common master image can be selected. The imaging features of the common master image can be reflected by the three factors.

(2) In the process of selecting the common master image, using the interferogram sequence with the removed gross error leads to selecting the most stable common master image.

(3) The procedure for weighing in the error analysis method is used to determine the influence of various factors in selecting the common master image. The results obtained using the error analysis method demonstrate smaller maximum, minimum, and standard deviation values and indicate better statistical properties than the other methods.

Owing to the imaging characteristics of the SAR data, the proposed method can be used for selecting the optimum common master image and can improve the quality of results in PS-InSAR. However, datasets from various remote sensing platforms present different imaging parameters. Thus, further research is required to ensure the application of the proposed technique to datasets from various platforms.

Acknowledgements

This work was supported by the Science and Technology Research Project of Jiangxi Provincial Education Department (Grant Nos. GJJ170468 and GJJ150557), State Key Laboratory Breeding Base of Nuclear Resources and Environment (East China Institute of Technology) (Grant No. NRE508), Jiangxi Province Education Science “13th Five-Year” Program (Grant Nos. 17YB070 and 17YB079), Liu Bao Jun Geoscience Foundation for Young Scientists (Grant No. DMSM2017010), Key Laboratory of Watershed Ecology and Geographical Environment Monitoring (NASG), Key Laboratory for Digital Land and Resources of Jiangxi Province East China University of Technology (Grant No. DLLJ201717).

This is an Open Access article distributed under the terms of the Creative Commons Attribution License



References

1. Ferretti, A., “InSAR permanent scatterer analysis reveals ups and downs in San Francisco Bay area”. *Transactions American Geophysical Union*, 85(34), 2004, pp.317-319.
2. Perrone, G., Morelli, M., Piana, F., Fioraso, G., Nicolò, G., Mallen, L., Cadoppi, P., Balestro, G., Tallone, S., “Current tectonic activity and differential uplift along the Cottian Alps/Po Plain boundary (NW Italy) as derived by PS-InSAR data”. *Journal of Geodynamics*, 66(5), 2013, pp.65-78.
3. Armaş, I., Mendes, D. A., Popa, R. G., Gheorghie, M., Popovici, D., “Long-term ground deformation patterns of Bucharest using multi-temporal InSAR and multivariate dynamic analyses: a possible transpressional system”. *Scientific Reports*, 7(3), 2017, pp. 437-462.
4. Rosi, A., Tofani, V., Tanteri, L., Tacconi Stefanelli, C., Agostini, A., Catani, F., Casagli, N., “The new landslide inventory of Tuscany (Italy) updated with PS-InSAR: geomorphological features and landslide distribution”. *Landslides*, 15(1), 2018, pp.1-15.
5. Ferretti, A., Rocca, F., “Permanent Scatterers in SAR interferometry”. *IEEE Transactions on Geoscience and Remote Sensing*, 39(1), 2001, pp.8-20.
6. Notti, D., Calò, F., Cigna, F., Manunta, M., Herrera, G., Berti, M., Meisina, C., Tapete, D., Zucca, F., “A user-oriented methodology for DInSAR time series analysis and interpretation: Landslides and Subsidence Case Studies”. *Pure and Applied Geophysics*, 172(11), 2015, pp.3081-3105.
7. Peduto, D., Cascini, L., Arena, L., Ferlisi, S., Fornaro, G., Reale, D., “A general framework and related procedures for multiscale analyses of DInSAR data in subsiding urban areas”. *ISPRS Journal of Photogrammetry and Remote Sensing*, 105(7), 2015, pp.186-210.
8. Frattini, P., Crosta, G. B., Rossini, M., “Activity and kinematic behavior of deep-seated landslides from PS-InSAR displacement rate measurements”. *Springer Science & Business Media*, 51(1), 2018, pp.1-18.
9. Fokker, P. A., Wassing, B. B. T., van Leijen, F. J., Hanssen, R. F., Nieuwland, D. A., “Application of an ensemble smoother with multiple data assimilation to the Bergermeer gas field, using PS-InSAR”. *Geomechanics for Energy and the Environment*, 5(3), 2016, pp.16-28.

10. Hooper, A., Zebker, H. A., Segall, P., et al., "A new method for measuring deformation on volcanoes and other natural terrains using InSAR persistent scatterers". *Geophysical Research Letters*, 31(L23611), 2004, pp.1-5.
11. Chen, Q., Ding, X., Liu, G., "Method for optimum selection of common master acquisition for PS-DInSAR". *Acta Geodaetica et Cartographica Sinica*, 36(4), 2007, pp.395-399.
12. Long, S. C., Liu, J. G., Li, T., Tang, C. H., "Method for optimum selection of common master acquisition for PS-DInSAR fusing GPS data". *Journal of Tongji University (Natural Science)*, 38(3), 2010, pp.453-458.
13. Kiseleva, E., Mikhailov, V., Smolyaninova, E., Dmitriev, P., Golubev, V., Timoshkina, E., Hooper, A., Samiei-Esfahany, S., Hanssen, R., "PS-InSAR monitoring of landslide activity in the Black Sea Coast of thecaucasus". *Procedia Technology*, 16(Supplement C), 2014, pp.404-413.
14. Tao, Q. X., Liu, G. I., "A new method to optimize and select common master images in PS InSAR". *Geomatics and Information Science of Wuhan University*, 36(12), 2011, pp.1456-1460.
15. Maghsoudi, Y., van der Meer, F., Hecker, C., Perissin, D., Saepuloh, A., "Using PS-InSAR to detect surface deformation in geothermal areas of West Java in Indonesia". *International Journal of Applied Earth Observation and Geoinformation*, 64(Supplement C), 2018, pp.386-396.
16. Zebker, H. A., Villasenor, J., "Decorrelation in Interferometric Radar Echoes". *IEEE Transactions on Geoscience and Remote Sensing*, 30(5), 1992, pp.950-959.
17. Kampes, B. M., Hassen, R. F., "Ambiguity resolution for permanent scatterer interferometry". *IEEE Transactions on Geoscience and Remote Sensing*, 42(11), 2004, pp.2446-2453.
18. Kampes, B. M. "Displacement parameter estimation using Permanent Scatterer Interferometry". *Master thesis of Delft University of technology*, USA, 2005, pp.18-32.
19. Kampes, B. M., Hanssen, R. F., Swart, L. M., "Strategies for nonlinear deformation estimation from interferometric stacks", In: *International Geoscience and Remote Sensing Symposium*, Sydney, Australia: IEEE, 2001, pp.2828-2831.
20. Chang, C. P., Yen, J. Y., Hooper, A., Chou, F. M., Chen, Y. A., Hou, C. S., Hung, W. C., Lin, M. S., "Monitoring of surface deformation in Northern Taiwan using DInSAR and PSInSAR techniques". *Terrestrial Atmospheric and Oceanic Sciences*, 21(3), 2010, pp.447-461.
21. Amato, V., Aucelli, P. P. C., Bellucci S. E., Cesarano, M., Incontri, P., Pappone, G., Valente, E., Vilardo, G., "Multidisciplinary approach for fault detection: Integration of PS-InSAR, geomorphological, stratigraphic and structural data in the Venafro intermontane basin (Central-Southern Apennines, Italy)". *Geomorphology*, 283(4), 2017, pp.80-101.
22. Zhang, H., Zeng, Q., Liu, Y., "The optimum selection of common master image for series of differential SAR processing to estimate long and slow ground deformation". In: *Geoscience and Remote Sensing Symposium, 2005. IGARSS '05*. Seoul, South Korea: IEEE, 2005, pp.4586-4589.
23. Wang, Z., Zhang, J. Q., "A method for selecting common master images in PS-InSAR". *Remote Sensing Information*, 1, 2013, pp.49-53.
24. Luo, H. B., He, X. F., "Method of time series differential interferogram common master image selection for PS-DInSAR". *Journal of Hohai University (Natural Sciences)*, 39(3), 2011, pp.344-347.
25. Pan, B., Shu, M., "Cluster analysis for selection of time series interferometric SAR imagery". *Journal of Applied Sciences*, 28(5), 2010, pp.501-506.
26. Liu, L. M., Gong, L. H., Yu, J., Chen, P. P., "A new optimization selection method of common master image for PS-InSAR interferometry". *Geomatics and Information Science of Wuhan University*, 40(12), 2015, pp.1594-1599+1612.
27. Liu, X. T., Cao, Q. X., Wang, S. P., Anastasia, C., "optimized method for selecting common master image in PS-DINSAR", *Journal of Engineering Science and Technology Review*, 11(1), 2018, pp.208-215.